Available online at www.sciencedirect.com
ScienceDirect
Ceramics International 35 (2009) 623–635
CERAMICS INTERNATIONAL
www.elsevier.com/locate/ceramint

The development of a thermodynamic model for Al_2O_3–MgO refractory castable corrosion by secondary metallurgy steel ladle slags

Jérôme Berjonneau, Pascal Prigent, Jacques Poirier *

Research Centre for Materials at High Temperature (CRMHT) 1D, Avenue de la Recherche Scientifique, 45071 Orléans Cedex 2, France

Received 12 July 2007; received in revised form 30 November 2007; accepted 22 January 2008
Available online 29 April 2008

Abstract

Alumina magnesia in situ spinel castables are used as ladle refractory lining in the steel industry. In contact with slag, they suffer degradations which limits their performance. The purpose of this article is to predict the thermochemical attack of a slag on alumina magnesia refractory using Factsage® thermodynamic modeling. To evaluate the reliability of the thermodynamic results, a validation step was carried out, which supported that the database was well adapted to the alumina magnesia spinel system. The corrosion phenomenon was then computed for a simple to a complete system to understand the mechanism and the influence of specific oxides. The model was also compared to corroded microstructures from a steel ladle to evaluate the contribution of each constituent in the castable. The aggregates of alumina react with slag to produce monomineral layers of lime aluminates (CA6 and CA2), while complex spinels (Mg, Fe, Mn)O (Fe_2, Al_2)O_3 are formed from the reaction of the slag with the matrix of the castable. Several oxides (MnO, FeO, Fe_2O_3) from the slag contribute to the formation of the spinel structures. The microstructures of refractories used in steel ladles confirm the main conclusions and the thermodynamic approach.

Keywords: C. Corrosion; D. Spinels; E. Refractories; Thermodynamic modeling

1. Introduction

Alumina-magnesia in situ spinel castables are used successfully in the steel industry, particularly in the impact pad of steel ladles (Fig. 1). These castables suffer degradations of thermochemical and thermomechanical origins which limit their performance. For instance, Fig. 2 shows the corrosion and the cracks of an alumina magnesia lining after use in a steel ladle.

The purpose of the present contribution is to obtain a better understanding of the corrosion of these refractories by slags from secondary metallurgy using a thermodynamic approach. The objectives are:

- to predict the compounds and the phases formed at high temperature at the thermodynamic equilibrium,
- to compare the theoretical results with microstructural observations carried out on corroded refractories from steel ladles.

This publication is divided into three parts:

- a description of the alumina-magnesia in situ spinel castable and of the ladle slags (mainly composed of lime and alumina),
- a presentation of the thermodynamic tools used and the validation of the calculations done within the scope of this study, and
- a modeling of the corrosion of alumina magnesia refractories by slags and a comparison of that model with corroded microstructures from field samples.

2. Description of Al_2O_3–MgO castables and of secondary metallurgy slags

Alumina magnesia in situ spinel castables are low cement content castables that contain alumina aggregates embedded in an alumina–lime matrix. Aggregates (comprising 70 wt.% of the castable) are made up of either tabular alumina or white corundum which range from a few millimetres to a few centimetres in particle size. The matrix is composed of alumina cement, fine grains of magnesia, microsilica, and fine to ultrafine particles of alumina (Fig. 3). In the alumina–magnesia

* Corresponding author. Tel.: +33 2 38 41 70 51; fax: +332 38 41 70 63.
E-mail address: jacques.poirier@univ-orleans.fr (J. Poirier).

0272-8842/$34.00
doi:10.1016/j.ceramint.2008.04.002

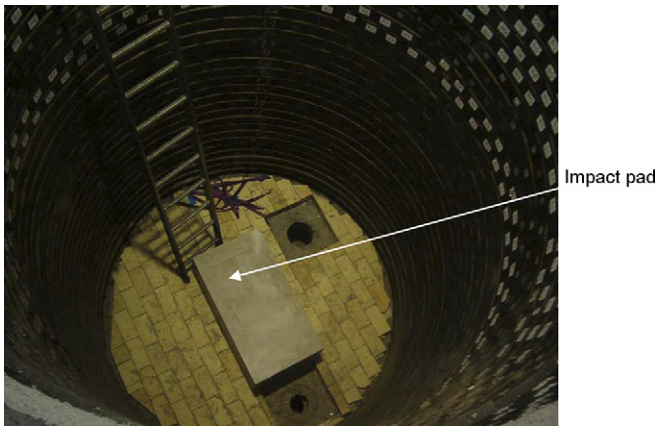

Fig. 1. Al_2O_3–MgO castable used in impact pad of a steel ladle.

castable, magnesia is present in matrix with a fine granulometry (around 10 μm). At working temperature, the magnesia totally reacts with fine alumina to form the spinel phase ($MgO–Al_2O_3$). In this study, the chemical influence of the minor phases is not considered. These castables have good thermomechanical properties, and above all, a high resistance to corrosion at elevated temperature. Table 1 presents the typical chemical analyses of several alumina magnesia castables.

Except when desulphurisation is practiced with a lime quasi-saturated slag, or when oxide inclusions are controlled by slag-steel reactions in speciality steels; the metallurgical function of steel ladle slags are limited to providing thermal insulation, protection from the atmosphere exposure, and catching deoxidation inclusions.

When molten steel is deoxidized using Al metal, the slags of secondary metallurgy are primarily composed of lime and

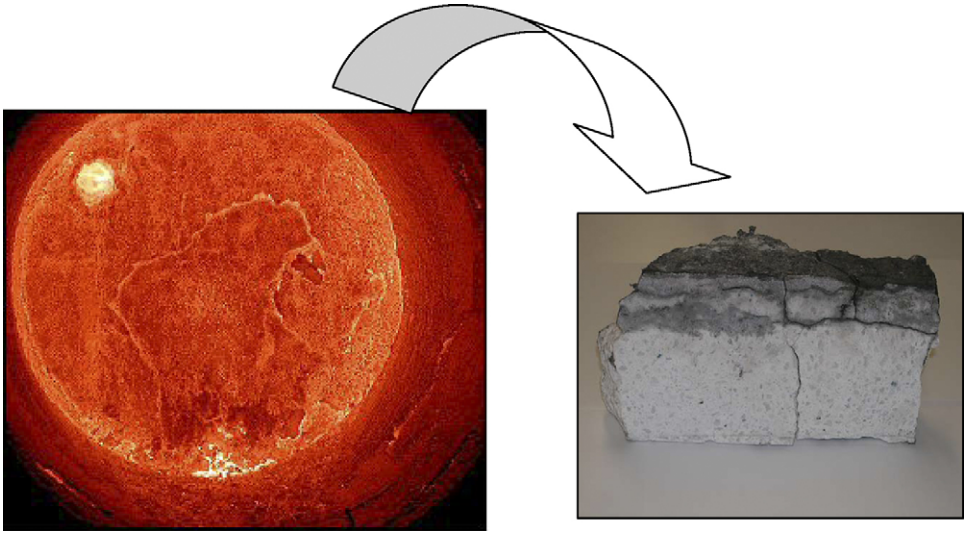

Fig. 2. Corrosion and cracks in an alumina–magnesia castable.

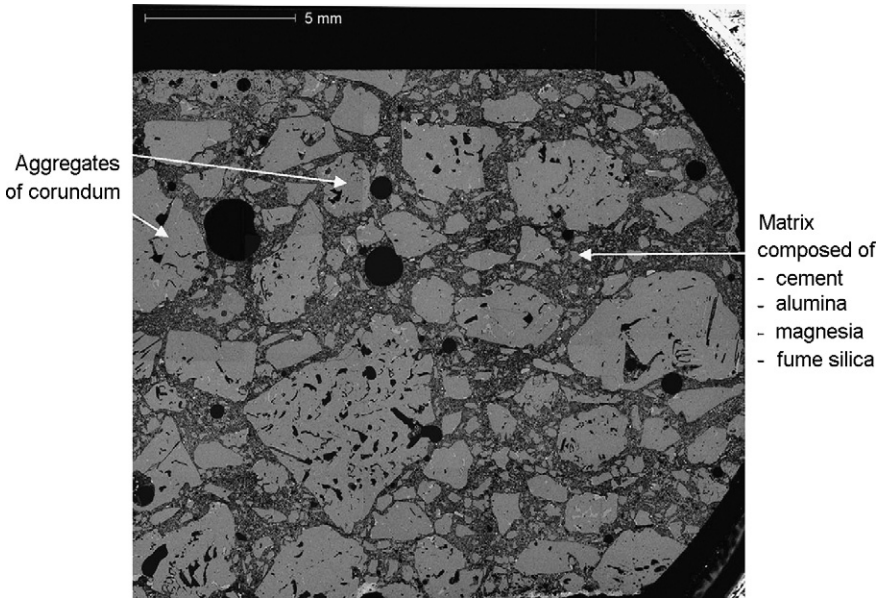

Fig. 3. Microstructure of an Al_2O_3–MgO castable.

Table 1
Chemical composition of some castables in weight percent (wt.%)

Castable	Al_2O_3	Fe_2O_3	Na_2O	SiO_2	CaO	MgO	TiO_2
A	94.1	0.2	0.2	0.5	1.3	3.6	0.1
B	93.1	0.5	0.3	0.7	1.2	4.0	0.1
C	91.9	0.1	0.2	2.1	1.0	4.6	0.0
D	91.5	–	–	0.9	1.7	5.0	–

Table 2
Simplified composition of the castables and the slags evaluated in this study

wt.%	Castable	Slag
Al_2O_3	95	50
CaO		50
MgO	5	
Al_2O_3	90.5	47.6
CaO		47.6
MgO	4.75	
SiO2	4.75	4.8
Al_2O_3	92.5	45
CaO	1.6	45
MgO	5	
SiO_2	0.9	
MnO		5
FeO		2.5
Fe_2O_3		2.5

alumina. Other slag oxides may be present in lower amounts, depending on the steel shop metallurgy practices and the steel grade. These slag oxides are:

- FeO_x (0–5 wt.%) and MnO (0–5 wt.%), which generally comes from the converter slag and from the oxidation of steel during casting in the ladle;
- MgO (3–10 wt.%), which originates mainly from the converter slag; and
- SiO_2 (0–10 wt.%), which comes from the converter slag or from silicon additions to the steel.

The corrosion of the alumina magnesia castables by model slags will be studied.

Table 2 gives the chemical compositions of these slags and these castables, which are composed of $CaO–Al_2O_3–MgO$, $CaO–Al_2O_3–MgO–SiO_2$, $CaO–Al_2O_3–MgO–SiO_2–FeO–Fe_2O_3–MnO$ oxides.

3. Description of the tools for thermodynamic calculations

The data and the calculations from thermodynamics are particularly suitable to understand the phenomena of corrosion. Calculations are based on the minimisation of free enthalpy of the system. It is thus possible to deduce the nature of the solid, liquid and gaseous phases, as well as their chemical composition and their reaction rate at the thermodynamic equilibrium. Liquidus and solidus temperatures as well as the solid and liquid phases can then be determined.

Calculations have been carried out using Factsage® (Version 5.4.1), a fully integrated database and software package developed jointly between Thermfact/CRCT (Montreal) and GTT-Technologies (Aachen). It consists of a series of modules that access and manipulate thermodynamic databases and perform various calculations. Factsage® is composed of two types of thermo-chemical databases-compounds (i.e. pure substances, over 4400 compounds) and real solutions. Using Factsage®, the following must be remembered:

- Compound databases are mainly for stoichiometric solid, liquid and gaseous species. For example, cristobalite and tridymite are included in a few non-stoichiometric compounds, such as FeO_x ($x = 0.947$).
- Solution data are for solid and liquid alloys, ceramics, salts, mattes, slags, etc. Data is stored in the form of Gibbs energy functions for the phase constituents and parameters for the excess Gibbs energy of mixing between the phases constituents. Factsage® supports several different solution models, including simple polynomial models such as the Redlich-Kister or the Legendre polynomial combined with different higher order extrapolations (Muggianu, Kohler, Toop), the quasichemical model, Pitzer parameters, and sublattice models [1].

Table 3
The number of liquid and solid phases and solutions involved in the calculation and references of the optimisation for the main binary systems

System	Number of liquid phases	Number of solid phases	Type of solutions	Optimisation
$CaO–Al_2O_3$	4	15	FToxid-SLAGA	[1]
CaO–MgO	4	7	FToxid-SLAGA FToxid-MeO_A (*I opt: possible 2-phases immiscibility*)	[2]
Al_2O_3–MgO	5	10	FToxid-SLAGA FToxid-SPIN FToxid-MeO_A	[3]
$MnO–Al_2O_3$	4	15	FToxid-SLAGA FToxid-MeO_A FToxid-AlSp	[4]
CaO–MnO	4	13	FToxid-SLAGA FToxid-MeO_A	[2]

The associated databases used in our study are: ELEM (elements thermodynamic database), FACT 53 (gas species, solid and liquid compounds thermodynamic database), and FT-oxid (compounds and solutions for oxides database).

The expected equilibrium phases were predicted using the "Equilibrium" module of Factsage®, considering as possible phases: the slag, several solid-solution phases (including spinel monoxide...), and all liquid (including the immiscible liquid

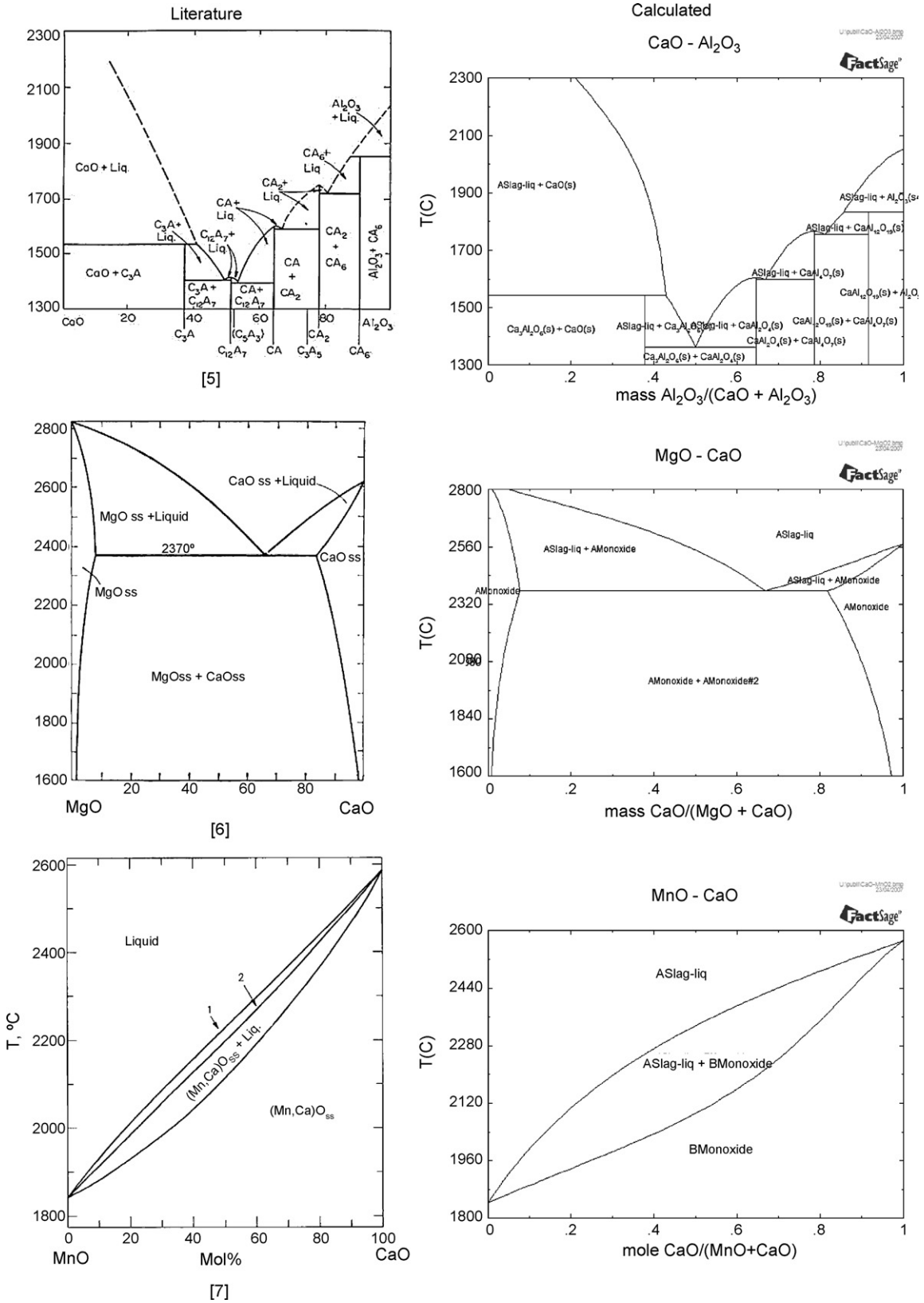

Fig. 4. $CaO–Al_2O_3$, MgO–CaO, MnO–CaO diagrams from the literature and from calculations.

Table 4
Liquidus and solidus temperatures from the literature and calculation for some compositions

System	Composition studied (wt.% ratio)	wt.% of slag	wt.% of refractory	Literature		Calculation	
				$T_{liquidus}$ (°C)	$T_{solidus}$ (°C)	$T_{liquidus}$ (°C)	$T_{solidus}$ (°C)
Al_2O_3–CaO	98.3/1.7	–	94.1	2007	1850	2040	1833
	50/50	90	–	1411	1406	1364	1362
	74.7/25.3	90	94.1	1710	1588.5	1746	1597
Al_2O_3–MgO	94.9/5.1	–	97.5	1980	1921	2004	2000
CaO–MgO	24.2/75.8	–	6.6	2688	2370	2704	2374
MnO–Al_2O_3	10/90	50	–	1988	1770	2021	1783
MnO–CaO	10/90	50	–	2525	2489	2538	2491

phase) and solid compounds between the inputs. Oxide compositions are entered as initial compositions in the sub-menu ''reactants'' of ''Equilib''.

The FToxid solution database contains data for pure oxides and oxide solutions of 20 elements. All the binary and ternary sub-systems have not been evaluated and optimised, nor are all composition ranges covered. Sub-systems which have not been evaluated and optimised have been assumed ideal, or have been approximated.

The FToxid database seems to be well adapted for our study. It contains the following major oxides: Al_2O_3, CaO, FeO, Fe_2O_3, MgO, SiO_2. All the binary and many ternary and quaternary sub-systems are more or less optimised. In particularly, for MnO, binary and many ternary sub-systems with the major oxides: Al_2O_3, CaO, FeO, Fe_2O_3, MgO and SiO_2 have been evaluated and optimised.

However, the corrosion of refractories by slag oxides is a complex phenomenon, and the interaction between these 7 oxides should be correctly calculated. In order to ensure the reliability and the pertinence of the results, it is necessary to validate first the thermodynamic calculation for simple systems. Consequently, the main sub-systems (binary and ternary) have been tested.

4. Validation of the thermodynamic calculations

A phase diagram is said ''optimised'' when all the data from the literature has been analysed, criticised, selected and used to

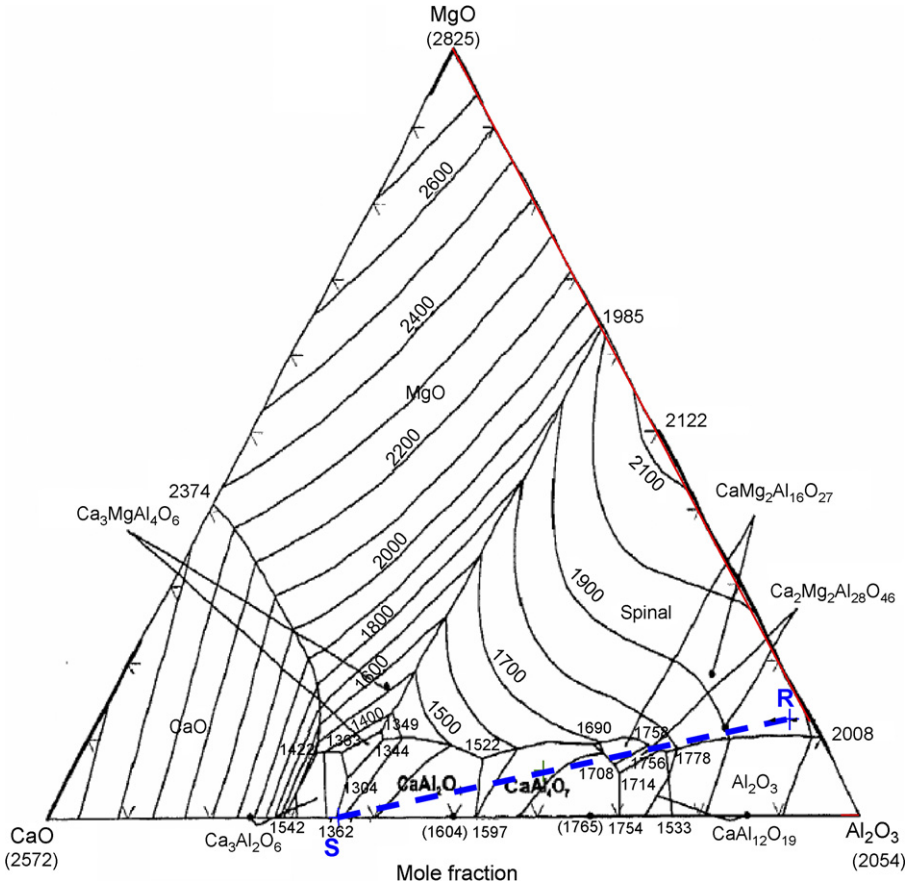

Fig. 5. Al_2O_3–CaO–MgO system: liquidus temperature (Factsage®).

determine the main parameters to calculate the phase diagrams. To validate the FToxid database, calculations have been done in the most pertinent binary and ternary diagrams of the Al_2O_3, CaO, FeO, Fe_2O_3, MgO, SiO_2 and MnO system.

4.1. Binary systems

The most important binary systems included within the scope of our study (Al_2O_3–CaO, Al_2O_3–MgO, CaO–MgO, MnO–Al_2O_3 and MnO–CaO) have been optimised by several authors. Characteristics of these 5 binary systems, with the number of liquids, solids and solutions taken into account for the equilibrium calculations are given in the Table 3 [2–5].

Phase diagrams of these systems were optimised by Factsage® and were found to reproduce in the same closely existing phase diagrams from the literature. Both types of diagrams are presented in Fig. 4 [6–8], to make comparison easier. The shape and the compounds found to exist in diagrams created using Factsage® and in the literature were found to be similar. Indeed the binary systems calculated are in agreement with the literature, and show their successful optimisation.

Calculations of liquidus and solidus temperatures have been carried out with different mixtures of slag and alumina magnesia refractories, and are compared with the literature (Table 4). The results are quite similar, with differences generally lower than 50 °C.

4.2. Ternary systems

The most important ternary systems have been studied and validate (Al_2O_3–CaO–MgO, Al_2O_3–CaO–MnO, SiO_2–CaO–MgO, SiO_2–CaO–Al_2O_3, SiO_2–MgO–Al_2O_3, Al_2O_3–CaO–Fe_2O_3...). Three typical compositions were computed using Factsage®: an alumina magnesia refractory, a slag, and a mixture (50 wt.% of refractory and 50 wt.% of slag), which were compared to the ternary system, and which had similar behaviour as the optimised diagram. For example, Al_2O_3–CaO–MgO, Al_2O_3–CaO–MnO systems are reported in following of this paper.

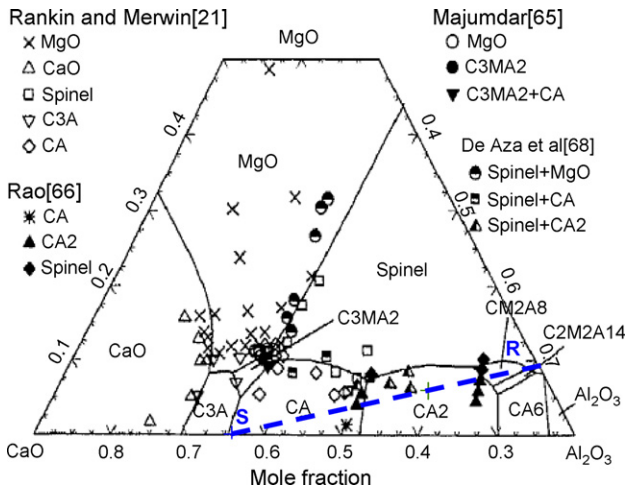

Fig. 6. Al_2O_3–CaO–MgO system: first crystalline phase (Factsage®).

Table 5
Liquidus temperature and first crystalline phase calculated for three typical compositions

Mole fraction	Refractory (R)	50% R + 50% S	Slag (S)
Al_2O_3	85.6	58.5	64.5
CaO	2.6	36	35.5
MgO	11.8	5.5	
$T_{liquidus}$ (°C)	1986	1688	1365
First crystalline phase	Spinel	$CaAl_4O_7$	$CaAl_2O_4$

4.2.1. Al_2O_3–CaO–MgO

The Al_2O_3–CaO–MgO system represents 90 wt.% of the slag and 99.1 wt.% of the components in the refractory composition. The liquidus surface and the primary crystallisation phase have been optimised [4] (Figs. 5 and 6). Calculations were been carried out for the three material compositions to determine the liquidus temperatures and the primary crystallisation phases, and to validate the optimised diagram (Table 5). This calculation also allowed us to identify the number of solid and liquid species involved and the solutions to be selected (Table 6). The liquidus temperatures and the first crystallisation phases from the calculations are in agreement with the optimised diagrams existing in the literature (Figs. 5 and 6: in mole fraction). From this data, the Factsage® modeled system is well optimised for these working conditions simulating steel refining.

However, other studies carried out by [9–12] showed the existence of $CaMg_2Al_{16}O_{27}$ and $Ca_2Mg_2Al_{28}O_{46}$ phases which exist across very limited ranges of composition, but have not been experimentally observed in this study. Therefore these species have been removed from the database and will not be considered in the following calculations.

4.2.2. Al_2O_3–CaO–MnO

This system represents 95 wt.% of the slag and 94.1 wt.% of the refractory composition, and has been optimised [13] in Fig. 7. As previously modeled, calculations have been carried out for the three defined compositions (Table 7). These calculations make it possible to identity the number of solid and liquid species involved and the solutions selected (Table 8). Calculations are in agreement with the optimised diagram, and showed this system is well optimised for the composition ranges studied.

To conclude the model validation, the calculations carried out in the main binary or ternary systems validate the optimised system in our composition range. The database for these calculations appear to simulate the Al_2O_3–CaO–MgO system,

Table 6
The number of solids and liquids and solutions involved in the calculation

Liquids	7
Solids	24
Solutions[a]	FToxid-SLAGA FToxid-SPIN FToxid-MeO_A

[a] Homogenous melt of several substances.

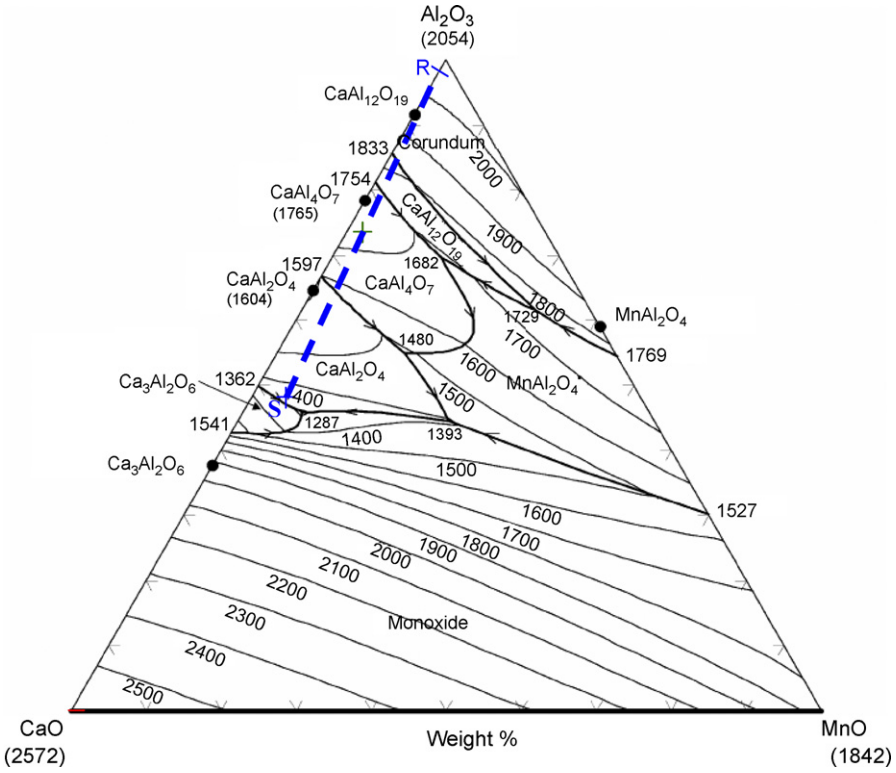

Fig. 7. Al_2O_3–CaO–MnO system liquidus temperature (Factsage®).

and will be used for calculation in more complex refractory/slag systems.

5. Modeling the corrosion of Al_2O_3–MgO castable by a CaO rich slag

The aim of this study is to simulate a real case of refractory attack by a slag. The approach is to apply the method from simplified cases (3 or 4 oxides) to real cases (Table 2), and to observe the role of the new oxides. For instance, the consequence of adding SiO_2 in the system will be observed.

5.1. Al_2O_3–CaO–MgO system

The first system studied is a simplified case in the ternary system Al_2O_3–CaO–MgO (Fig. 8). The refractory is made up of 95 wt.% Al_2O_3 and 5 wt.% MgO and the slag with 50 wt.% Al_2O_3 and 50 wt.% CaO. All possible proportions between these two compositions will be studied as a function of the reaction rate $\langle A \rangle$ at 1600 °C. The reaction rate $\langle A \rangle$ is defined by the ratio: (R)/[(S) + (R)] with (S) + (R) = 1 (R is the refractory and S the slag). All the other parameters (temperature, pressure) are constant.

5.1.1. Calculations

The result (Fig. 9) can be divided into different zones which are discussed from the refractory to the slag in the following part.

- For the highest $\langle A \rangle$: $0.88 < \langle A \rangle < 1$: three phases are obtained (Al_2O_3, spinel and slag). The slag phase is in contact with two solid phases: Al_2O_3 and spinel. The amounts of Al_2O_3 and spinel decrease as $\langle A \rangle$ decreases and the amount of slag increases.
- For $0.86 < \langle A \rangle < 0.88$: the system is composed of two phases, Al_2O_3 and the slag. Spinel is no longer present, and MgO is completely dissolved into the slag phase.
- For $0.78 < \langle A \rangle < 0.86$: Al_2O_3 reacts with slag producing CaO–$6Al_2O_3$ (CA6). In this range, the composition of the slag is constant.

Table 7
Liquidus temperature and first crystalline phase calculated for three typical compositions

Wt.%	Refractory (R)	0.5 R + 0.5 S	Slag (S)
Al_2O_3	98	72.7	47.4
CaO	2	24.7	47.4
MnO		2.6	5.2
Tliquidus (°C)	2038	1723	1321
First crystalline phase	Al_2O_3	$CaAl_4O_7$	$CaAl_2O_4$

Table 8
Number of solids and liquids and solutions involved in the calculation

Liquids	6
Solids	25
Solutions	FToxid-SLAGA
	FToxid-AlSp
	FToxid-MeO_B

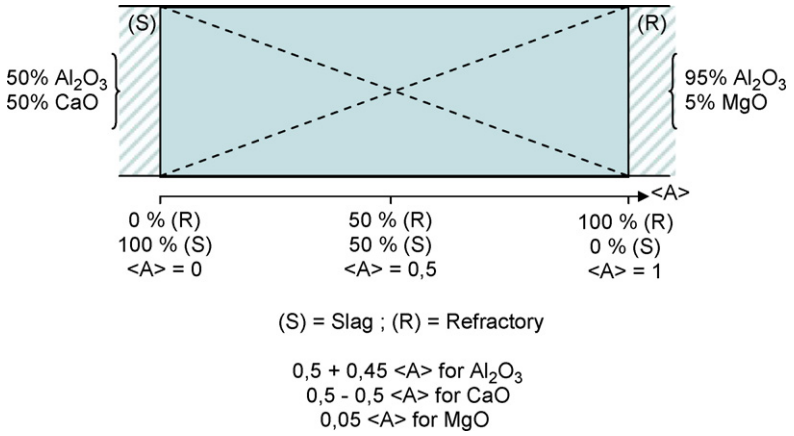

Fig. 8. Interaction between slag and refractory as a function of ⟨A⟩.

- For $0.72 < \langle A \rangle < 0.78$: this zone is composed of two phases, CA6 and the slag phase. The composition of the slag changes.
- For $0.6 < \langle A \rangle < 0.72$: this domain is composed of three phases: slag, CA6 and CA2. CA6 reacts completely with the slag to produce CA2.
- $0.39 < \langle A \rangle < 0.6$: two phases are formed: CA2 and the slag.
- For values lower than $\langle A \rangle < 0.39$, the slag is the only phase formed.

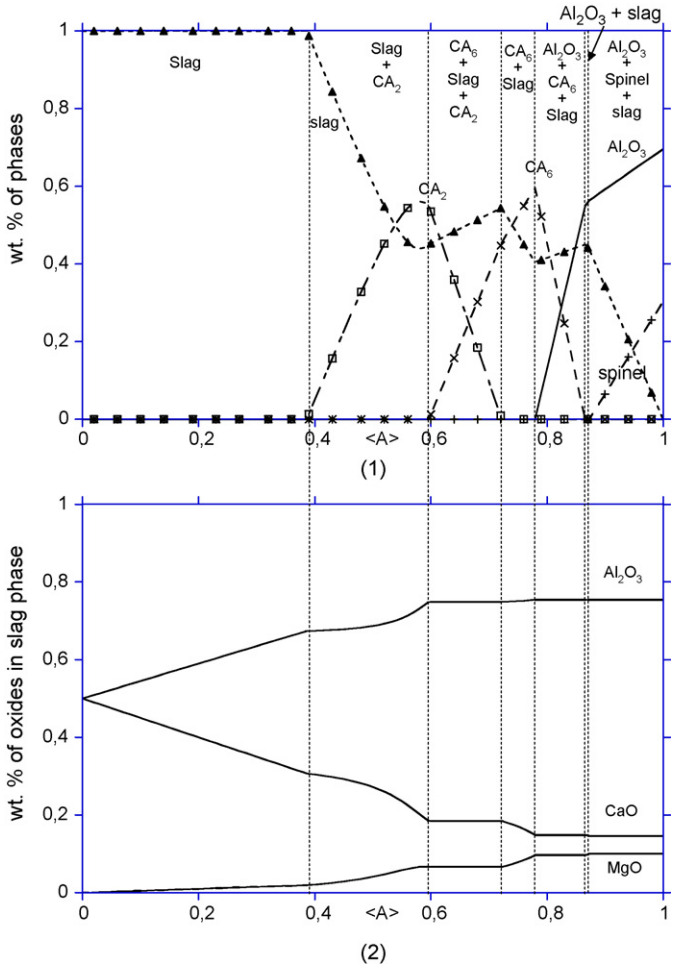

Fig. 9. Weight percent of the phases formed (1) and of the slag composition (2) as a function of ⟨A⟩.

The thermodynamic calculation shows the species which could be formed in the Al_2O_3–CaO–MgO system: Al_2O_3, spinel, CA6, CA2 and slag. Spinel and CA6 are formed for high values of ⟨A⟩ and CA2 is formed for low values of ⟨A⟩, when the system becomes low in alumina.

This study allows us to know the species which may coexist. For instance, CA2 may not coexist with alumina or with spinel.

It is interesting to correlate the reaction rate of the system with the evolution of the slag (its amount and its composition). Afterwards, when the system is composed of one solid and the slag, the amount of slag increases with decreasing ⟨A⟩ and its composition varies. When the system is composed of the slag and two solids, the composition of the slag becomes steady in agreement with the phase rule of Gibbs (see Section 5.1.2). The amount of the slag decreases to produce a new species except for the first zone ($0.88 < \langle A \rangle < 1$), where alumina, spinel and slag exist. The liquid phase could be considered as the driving force behind the corrosion phenomenon. Indeed, in the presence of one solid phase, the composition of the slag varies

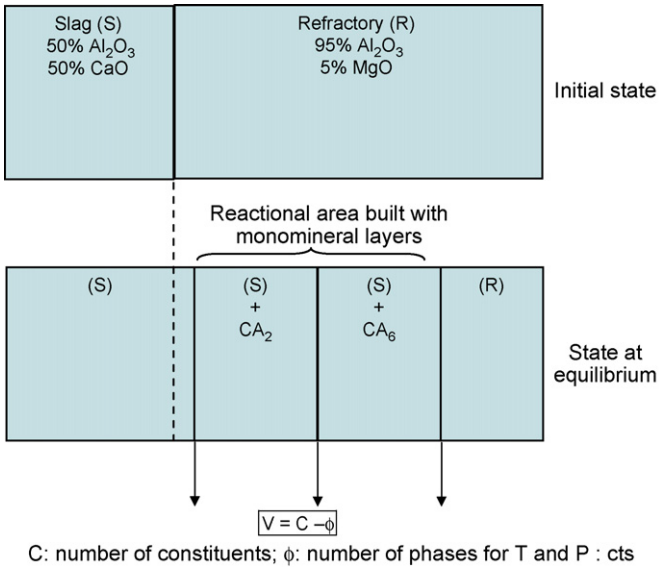

Fig. 10. Scheme of different monomineral zones at the initial and final states of the theoretical approach.

to reach a specific composition needed to produce a second solid with the solid phase in presence.

5.1.2. Interpretation

The degree of freedom V (variance) of the system is given by the phase rule of Willard Gibbs. Eq. (I) gives the usual mathematical form of the phase rule:

$$V = C + 2 - \phi \quad \text{(I)}$$

- C: number of components of the system.
- ϕ: number of the phases present at equilibrium.
- 2: number of environmental factors (temperature and pressure).

When the temperature and the pressure are fixed, the Gibb's phase rule reduce to the Eq. (II):

$$V = C - \phi \quad \text{(II)}$$

The phase rule applies only to equilibrium states of a system, which require both homogeneous equilibrium within each phase and heterogeneous equilibrium between co-existing phases. The phase rule does not depend on the nature and amounts of the phases present, but only on their numbers; nor does it give information concerning rates of reactions. Non-conformity with the phases rule is proof that equilibrium conditions do not exist.

When a system is composed of 3 constituents, the variance (V) is equal to: $V = 3 - \phi$. In this case, the phase number must be lower or equal to 3. Two scenarios are possible and are described below.

- At the solid–solid interfaces, a liquid phase is in contact between two solids. The number of phases is then equal to 3 ($\phi = 1$ liquid + 2 solid = 3) and the variance to 0 ($V = 0$). It means that the composition of the liquid is constant in this domain.
- In a reaction zone, the liquid phase is in contact with one solid only. The phase number is then equal to 2 ($\phi = 1$ liquid + 1 solid = 2) and the variance is equal to 1 ($V = 1$). This means that the composition of the liquid is not constant.

The initial and the final states of corrosion based on thermodynamic calculations are shown in Fig. 10. The refractory reacts with the slag to produce CA6 and CA2 monomineral zones separated by boundaries which move gradually. The thickness of each zone depends on the kinetic factors.

A succession of three- and two-phase layers as a function of $\langle A \rangle$ are observed. CA6 is richer in alumina than CA2, and is calculated to be closer to the alumina layer.

When slag is in contact with two solid species (the system is then composed of three phases), the variance is equal to 0 and the composition of the slag is steady (Fig. 9(2)). In contrast, when the slag is in contact only with one phase, the variance is higher than 0. The result shows the composition of the slag is no longer constant.

5.2. Al_2O_3–CaO–MgO–SiO_2 system

A small quantity of silica was added (5 wt.%) in the Al_2O_3–CaO–MgO–SiO_2 system and the solid species and the composition of the liquid phase plotted as a function of $\langle A \rangle$ (Fig. 11).

This system is composed of 4 constituents, with the variance equal to: $V = 4 - \phi$. The phase number must be lower than or equal to 4, with the theoretical calculations indicating the coexistence of at most three phases. In this example, the variance is then always higher than zero and the slag phase is never constant in composition.

The result can be divided into different zones, as shown in Fig. 11, and discussed below:

- For the highest $\langle A \rangle$: $0.88 < \langle A \rangle < 1$: three phases are obtained. The slag phase is in contact with two solid phases: Al_2O_3 and spinel. The amount of Al_2O_3 and spinel decrease as $\langle A \rangle$ decreases, while the amount of the slag increases.
- For $0.79 < \langle A \rangle < 0.88$: the system is composed of two phases: Al_2O_3 and the slag. Spinel is no longer formed. MgO is then completely dissolved in the slag phase.
- For $0.73 < \langle A \rangle < 0.79$: Al_2O_3 reacts with slag producing CaO–$6Al_2O_3$ (CA6). The composition of the slag is almost steady.

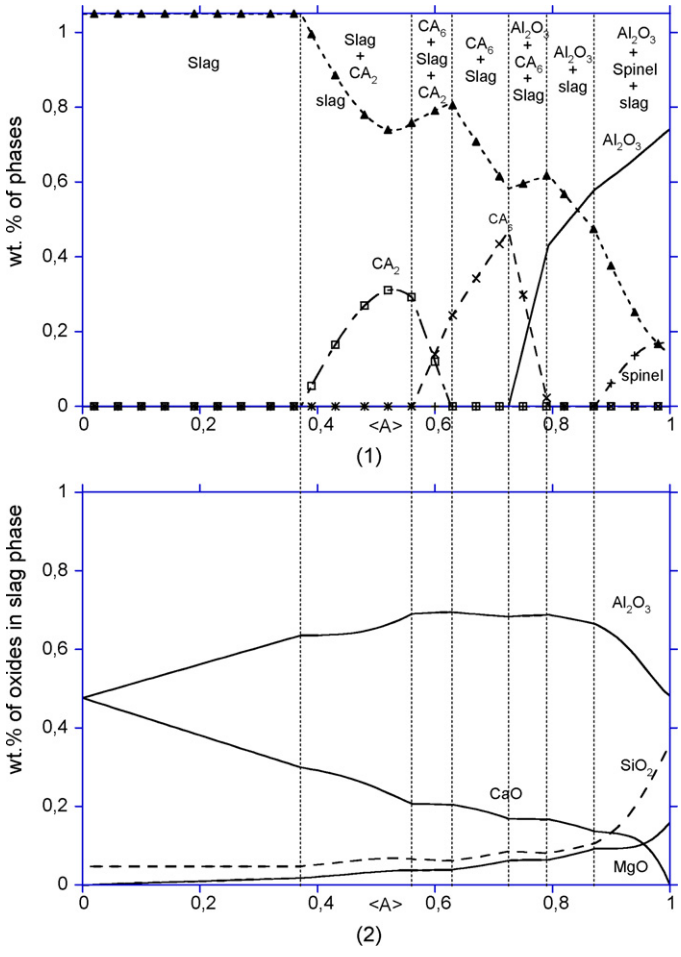

Fig. 11. Weight percent of the phases formed (1) and of the slag composition (2) as a function of $\langle A \rangle$.

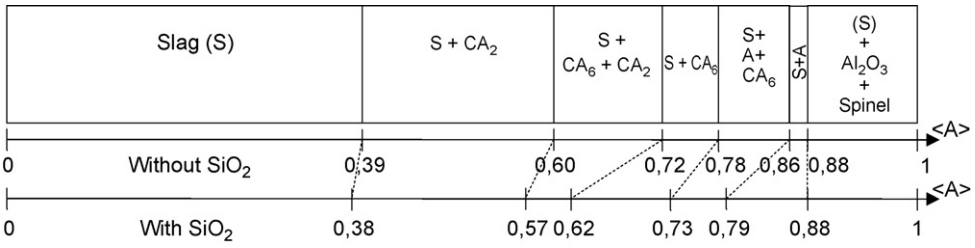

Fig. 12. ⟨A⟩ boundaries between the different layers with and without SiO_2.

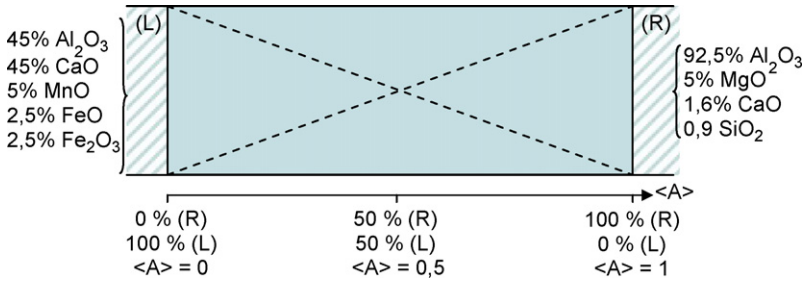

Fig. 13. Simulation model of the interaction between total slag and refractory as a function of ⟨A⟩.

- For $0.62 < \langle A \rangle < 0.73$: this zone is composed of two phases: CA6 and the slag phase. The composition of the slag is not steady any more.
- For $0.57 < \langle A \rangle < 0.62$: there are three phases: the slag, CA6 and CA2. CA6 reacts completely with the slag to produce CA2. The composition of the slag is almost steady again.
- $0.38 < \langle A \rangle < 0.57$: two phases are formed: CA2 and the slag.
- For values lower than $\langle A \rangle < 0.38$, the slag is the only phase formed.

Except for the first zone ($0.88 < \langle A \rangle < 1$) where alumina, spinel and slag exist, the composition of the slag is almost steady in the zones containing 3 phases, even if the variance is not equal to 0. It means that only a narrow range of slag composition is suitable to produce the lime–aluminate phases (CA*x*).

Even if the slag is now made up of four oxides (Al_2O_3–CaO–MgO–SiO_2) with a silica level lower than 5 wt.%, this system has the same behaviour as the ternary system previously described with a succession of three- and two-phase layers. However the widths of the layers as a function of ⟨A⟩ are not the same with and without SiO_2. The ⟨A⟩ boundaries between each layer are shown in Fig. 12. In general, the addition of SiO_2 widens the two-phase layers and makes the three-phase layers narrower.

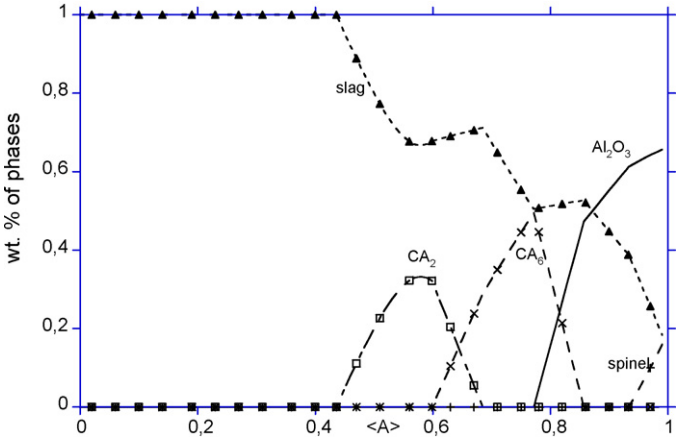

Fig. 14. Weight percent of the phases formed as a function of ⟨A⟩.

5.3. Al_2O_3–CaO–MgO–MnO–FeO–Fe_2O_3 system

A simulation model is showed in Fig. 13. In a first step, all the constituents are taken into account. The amount of each phase is plotted as a function of ⟨A⟩ (Fig. 14). This system is not really different from the Al_2O_3–CaO–MgO–SiO_2 system. As previously described, alumina and spinel are formed for the highest values of ⟨A⟩. Alumina then reacts with slag producing CA6 and CA2 subsequently with decreasing ⟨A⟩.

6. Influence of the microstructure on corrosion

Alumina magnesia in situ spinel castables are heterogeneous materials. The resultant microstructure consists of large alumina aggregates and a finer, more porous intergranular matrix (Fig. 15). Consequently, to understand the corrosion mechanisms, the microstructure (in particular, composition grains and bond phases) should be examined. The higher porosity and fine texture of the matrix make it more reactive than the aggregates. In Fig. 16, the castable is infiltrated by the slag to a thickness of about 5 mm. The reaction between the

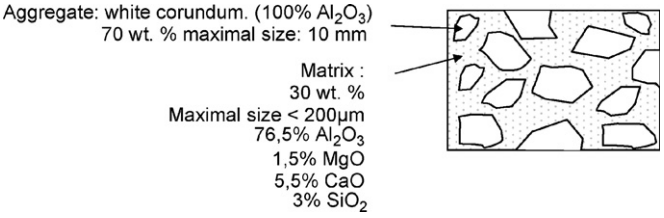

Fig. 15. Alumina–magnesia castable.

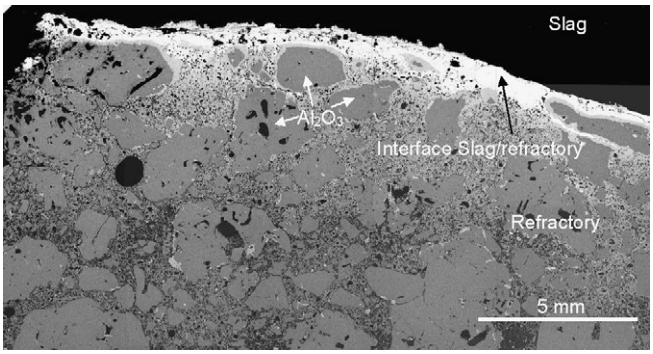

Fig. 16. Microstructure of an Al_2O_3–MgO castable corroded by a lime rich slag in a steel ladle.

slag and the matrix produces new phases. The grains in the corrosion zone are not attacked except on their surface, where a new phase appears.

Calculations will focus on the interaction between the slag and the constituents of the refractory (either the matrix or the aggregates).

The objectives of these calculations are:

- to analyse the specific contribution of each part of the castable in contact with slag,
- to correlate the result of the simulation with a real microstructure (Fig. 16),
- to confirm the formation of CA6 and CA2 phases from the alumina aggregates, and
- to better understand the formation and the nature of the spinel.

6.1. Interaction between slag and alumina aggregates

The amount of the phases formed is plotted as a function of ⟨A⟩ (Fig. 17). For the highest ⟨A⟩, Al_2O_3 is formed with CA6, with the amount of Al_2O_3 decreasing and of CA6 increasing when ⟨A⟩ decreases (the amount of slag increases). Further decreases in ⟨A⟩ cause Al_2O_3 to disappear and for CA2 to form. The amount of CA2 increases while the amount of CA6 decreases until it completely disappears. Finally, CA2 is the last compound formed with decreasing ⟨A⟩, which decreases with further decreases in ⟨A⟩ until it is replaced by slag.

To facilitate the explanation of the formation of these monomineral layers, a schematic representation is drawn (Fig. 18).

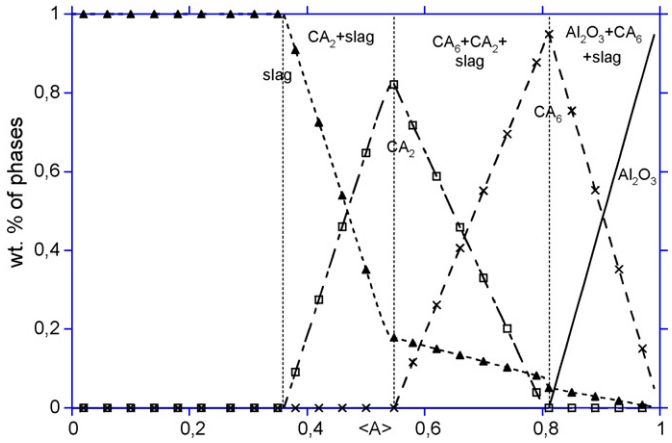

Fig. 17. Interaction between slag and alumina aggregates: weight % of the phases formed as a function of ⟨A⟩.

For the highest ⟨A⟩, alumina reacts with slag producing 6 ⟨Al_2O_3⟩ + [CaO] → ⟨CA6⟩ (where ⟨ ⟩ means "in the solid state" and [ ] means "dissolved in liquid phase") (Fig. 18 (2)). This reaction goes on as long as the slag is in contact with alumina, that is to say until the layer of CA6 completely surrounds the alumina in contact with slag. Then, CA6 plays the role of a diffusion barrier which slows down the penetration of the liquid species.

CA6 becomes the only solid phase in contact with the slag. Its amount respectively increases, then decreases as ⟨A⟩ decreases. As previously explain in Section 5.1.1, the liquid phase could be considered as the driving force behind the corrosion phenomenon. By yielding CA6 with alumina, the slag composition varied, the CA2 phase precipitates and becomes steady in contact with CA6.

In the following range of ⟨A⟩, the slag reacts with CA6, decreasing it and producing CA2: ⟨CA6⟩ + 2 [CaO] → 3 ⟨CA2⟩ (Fig. 18 (3)). CA2 is formed as long as CA6 is in contact with the slag (from Fig. 18 (3 and 4)). CA2 is the last solid phase formed in contact with the slag phase.

This result can be used to explain SEM microstructures observed in a corroded refractory sample from a steel ladle impact pad (Fig. 19). The microstructures experimentally observed in Figs. 16 and 19(a) show the layering of alumina, CA6, CA2 and slag. The black zone [on the right side of Fig. 19a] corresponds to an electrofused alumina aggregate. The next layer corresponds to CA6, and the following one to

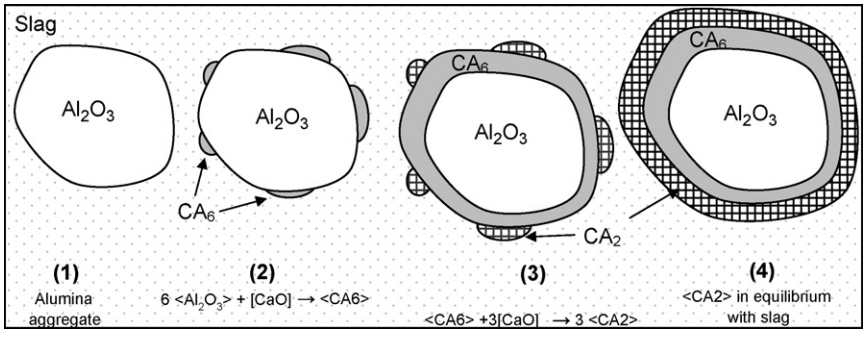

Fig. 18. Schematic representation of the interaction between aggregate and slag. ⟨ ⟩: means "in the solid state"; [ ]: means "dissolved in a liquid phase".

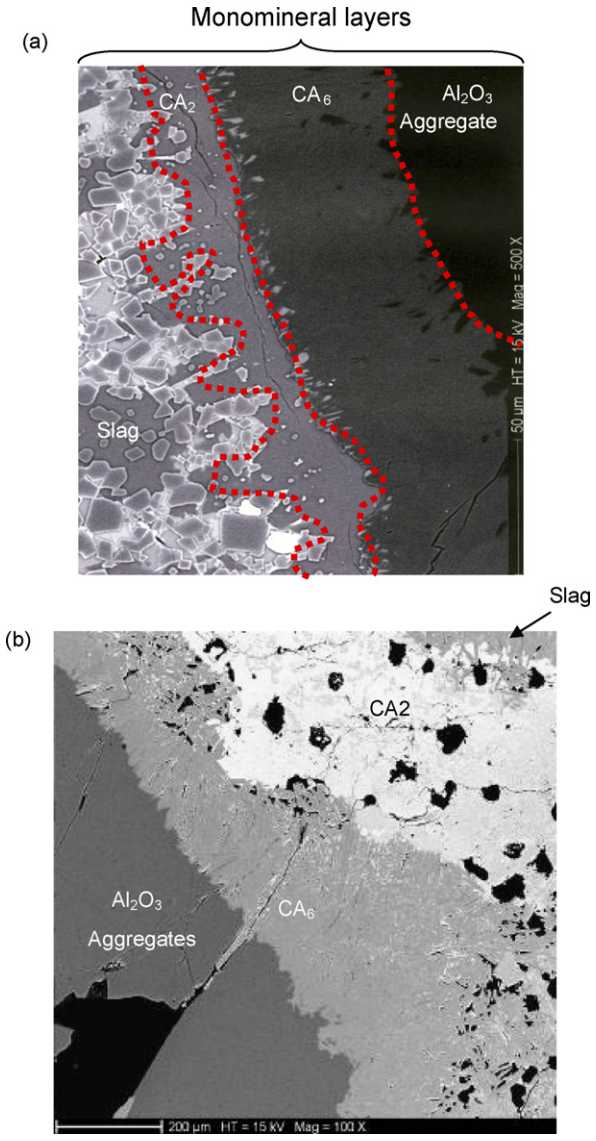

Fig. 19. SEM observation of two different microstructures (a) and (b) of an alumina aggregate after attack by slag.

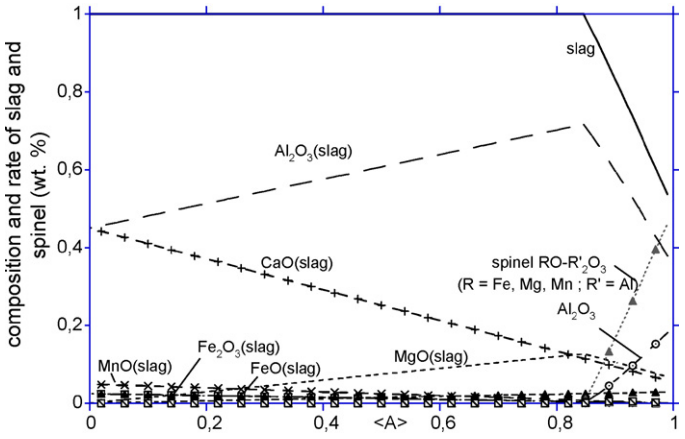

Fig. 20. Interaction between slag and matrix: weight % of the phases formed as a function of ⟨A⟩.

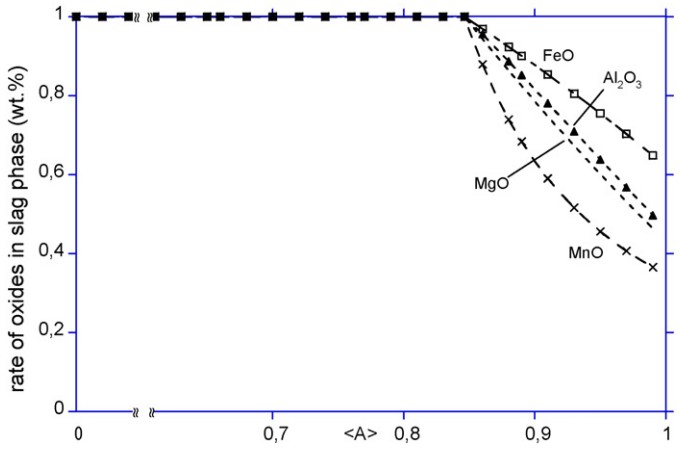

Fig. 21. Interaction between slag and matrix: weight % of FeO, Al_2O_3, MgO and MnO in the liquid state as a function of ⟨A⟩.

CA2. The microstructure is then composed of a succession of monomineral layers. The texture and the shape of the layers clearly indicate that the crystals are precipitated from a liquid. Both CA6 from the first layer and CA2 from the second layer show well-formed crystals. The corrosion of alumina aggregates can be explained as a dissolution–precipitation process inside a liquid phase. This is in agreement with the calculation from Factsage® (Fig. 17). Indeed, the local thermodynamical approach shows and explains the succession of monomineral layers experimentally observed.

6.2. Interaction between slag and matrix

The simulation takes into account only the slag and the matrix of the castable. The solid phases formed between the slag and refractory interactions for the highest ⟨A⟩ are alumina

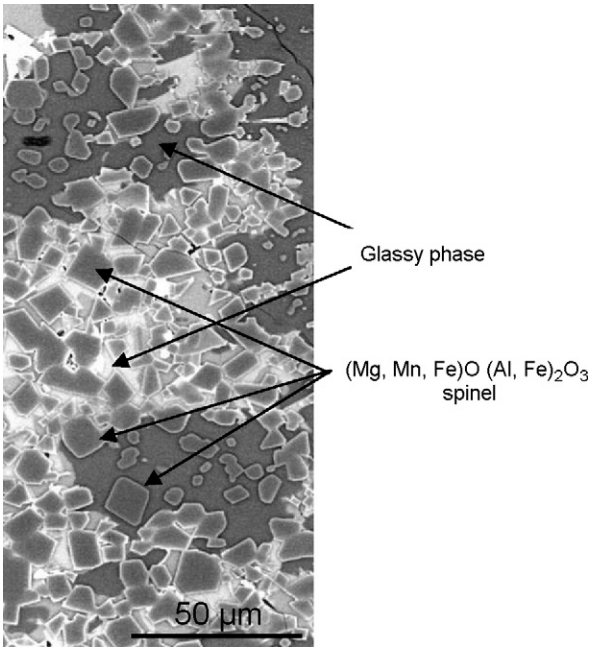

Fig. 22. SEM observation of the microstructure of the matrix after attack by a slag.

and spinel RO − R'_2O_3 (Fig. 20), composed of FeO, MgO, MnO (for RO) and Al_2O_3 for R'_2O_3. These oxides, which come from the slag, are ''trapped'' in the spinel structure. This hypothesis is confirmed in Fig. 21 which shows the amount of these four species in liquid state as a function of ⟨A⟩. A strong decrease is observed from the highest ⟨A⟩ which results from the contribution of these oxides to the formation of the solid phases. Microstructures resulting from the interaction between spinel and slag are observed by SEM in Fig. 22. Crystals and glass are formed in the matrix. The crystals' size of around 10 μm and their square shape clearly indicate that spinel have been crystallised at high temperature (1600–1650 °C) in a liquid phase. The EDS analyses indicate that these crystals contain iron and manganese oxides which have diffused in the spinel into substitution of the magnesia.

7. Conclusion

A thermodynamic modeling was applied to alumina magnesia castables used in the secondary metallurgy slags and their steel making applications, and data compared to post-mortem evaluation of actual samples. The tools for thermodynamic calculations have pointed out the need to validate the database used, and binary and ternary systems from the literature were compared with the calculations. The database was shown to be well adapted for the composition ranges studied.

Thermodynamic calculations were then carried out from simple systems to complicated slag systems (containing MnO, FeO and Fe_2O_3 addition to Al_2O_3, CaO, MgO and SiO_2) as a function of the reaction rate ⟨A⟩. The first one (included in the ternary system Al_2O_3–CaO–MgO) shows the formation of a slag and four solid phases: alumina, CA6, CA2 and spinel; which could co-exist indifferent amounts in a system made up of three and two-phase layers. The behaviour of the liquid phase (as a function of the variance) indicated it is the driving force behind the corrosion phenomenon. When the liquid phase is in contact with two solids (the variance is then equal to 0), in the simple systems, the composition of the liquid phase is steady and its amount decreased. When the slag is in contact with one solid, the variance equals 1, and the composition of the liquid phase varies in order of reaching a typical composition to produce a second solid.

SiO_2 additions were found to influence solid equilibrium materials and quantities. Even if the behaviour of the system was similar to the simpler systems studied, the boundary layers are not the same: the two-phase layers become wider and the three phase layers narrower, with SiO_2 increases causing the quantity of solid phases to decrease, and the liquidus temperature to decrease. At a constant temperature, the amounts and the range of formation of the solid phases decreased with increases in SiO_2 quantity.

The complete slag/refractory system for MgO/Al_2O_3 and slag is thermodynamically modeled and was found to explain post-mortem observation. The main results are:

- CA6 and CA2 result directly from the corrosion of the aggregates of alumina with slag. The succession of these monomineral layers are confirmed by the SEM microstructure observations.
- Spinel results from the reaction of the MgO/Al_2O_3 matrix with slag. Al_2O_3, FeO, MgO and MnO from slag form spinel solid solutions. At the same time the slag is enriched in alumina and lime, and became impoverished in MnO and FeO.

To conclude, the thermodynamic modeling was in good agreement with microstructure, and explained the mechanism of slag corrosion on the refractory grain. Modeling accounted for the role played by each oxide of the slag and refractory. In contact to the slag, the aggregate of alumina reacts with the lime of the slag to produce lime aluminates (CA6 and CA2). First, a layer of CA6 was formed caused by a reaction of the alumina grains with lime in the slag. When the aggregate were completely covered with the layer of CA6 (causing no contact with the slag), CA6 reacted with lime–alumina slag to produce CA2. At the same time, the matrix reacted with slag to produce spinel. Some oxides from the slag (Al_2O_3, FeO, MgO, MnO) take part in the formation of the spinel, and become part of the structure.

References

[1] C.W. Bale, P. Chartrand, S.A. Degterov, G. Eriksson, K. Hack, R. Ben Mahfoud, J. Melançon, A.D. Pelton, S. Petersen, Factsage thermochemical software and databases, Calphad 26 (2) (2002) 189–228.
[2] G. Eriksson, A.D. Pelton, Critical evaluation and optimization of the thermodynamic properties and phase diagrams of the CaO–Al_2O_3, Al_2O_3–SiO_2 and CaO–Al_2O_3–SiO_2 systems, Metall. Trans. 24B (1993) 807–816.
[3] P. Wu, G. Eriksson, A.D. Pelton, Critical evaluation and optimization of the thermodynamic properties and phase diagrams of the CaO–FeO, CaO–MgO, CaO–MnO, FeO–MgO, FeO–MnO and MgO–MnO systems, J. Am. Ceram. Soc. 76 (1993) 2065–2075.
[4] I.-H. Jung, S. Decterov, A.D. Pelton, Critical thermodynamic evaluation and optimization of the MgO–Al_2O_3, CaO–MgO–Al_2O_3 and MgO–Al_2O_3–SiO_2 systems, J. Phase Equilib. 25 (2004) 329–345.
[5] G. Eriksson, P. Wu, A.D. Pelton, Critical evaluation and optimization of the thermodynamic properties and phase diagrams of the MgO–Al_2O_3, MnO–Al_2O_3, FeO–Al_2O_3, Na_2O–Al_2O_3 and K_2O–Al_2O_3 systems, Calphad J. 17 (1993) 189–206.
[6] F.M. Lea, C.H. Desch, The Chemistry of Cement and Concrete, second ed., Edward Arnold & Co., London, 1956, p. 52.
[7] R.C. Doman, J.B. Barr, R.N. McNally, A.M. Alper, J. Am. Ceram. Soc. 46 (7) (1963) 314.
[8] D.S. Kamenetskaya, T.T. Riskiev, B.L. Revzin, L.M. Ni, Izv. Akad. Nauk SSSR, Neorg. Mater. 21 (3) (1985) 422–425;
D.S. Kamenetskaya, T.T. Riskiev, B.L. Revzin, L.M. Ni, Inorg. Mater. (Engl. Transl.) 21 (3) (1985) 356–359.
[9] M. Göbbels, E. Woermann, J. Jung, The Al-rich part of the system CaO–Al_2O_3–MgO: Part I: phase relationships, J. Solid State Chem. 120 (1995) 358–363.
[10] N. Iyi, M. Göbbels, Y. Matsui, The Al-rich part of the system CaO–Al_2O_3–MgO: Part II: structure refinement of two new magnetoplumbite-related phases, J. Solid State Chem. 120 (1995) 364–371.
[11] A.H. De Aza, P. Pena, S. De Aza, Ternary-system Al_2O_3–MgO–CaO:I: primary phase field of crystallization of spinel in subsystem $MgAl_2O_4$–$CaAl_4O_7$–CaO–MgO, J. Am. Ceram. Soc. 82 (1999) 2193–2203.
[12] A.H. De Aza, J.E. Iglesias, P. Pena, S. De Aza, Ternary-system Al_2O_3–MgO–CaO:II: phase relationships in the subsystem Al_2O_3–$MgAl_2O_4$–$CaAl_4O_7$, J. Am. Ceram. Soc. 83 (2000) 919–927.
[13] Y.-B. Kang, I.-H. Jung, S. Decterov, A.D. Pelton, H.-G. Lee, Thermodynamic evaluation and optimization of the CaO–MnO–SiO_2 and CaO–MnO–Al_2O_3 systems, ISIJ Int'l 44 (6) (2004) 965–974.